EMBEDDED FIBER-OPTIC SENSORS FOR IN-PILE APPLICATIONS*

Christian Petrie, Niyanth Sridharan
Oak Ridge National Laboratory
P.O. Box 2008, Oak Ridge, TN 37831
petriecm@ornl.gov; sridharann@ornl.gov

Curtis Frederick, Travis McFalls, Sudarsanam Suresh Babu
Department of Mechanical, Aerospace and Biomedical Engineering
University of Tennessee, Knoxville
2712 Neyland Drive, Knoxville, TN 37996
cfreder2@vols.utk.edu; tmcfalls@vols.utk.edu; sbabu@utk.edu

Adam Hehr, Mark Norfolk
Fabrisonic LLC
1250 Arthur E Adams Dr, Columbus, OH 43221
ahehr@fabrisonic.com; mnorfolk@fabrisonic.com

John Sheridan
Sheridan Solutions LLC
745 Woodhill Dr, Saline, MI 48176
johns@sheridansolutions.com

ABSTRACT

Qualification and commercialization of new nuclear fuels and materials requires a comprehensive set of data regarding behavior under irradiation. There are currently very limited options for in-situ monitoring of material evolution during irradiation due to the extremely harsh environment (i.e., high temperatures and intense radiation) of materials test reactors. This paper describes work being performed at Oak Ridge National Laboratory to embed metal-coated fiber-optic sensors into in-core irradiation experiments to enable measurement of radial dimensional changes and spatially distributed temperature and strain. Some critical issues that must be addressed before embedded fiber optics can be deployed in-core include (1) embedding of metal-coated fibers without failure or prohibitively large signal attenuation, (2) embedding in curved channels to allow for radial dimensional measurements, and (3) demonstrating that embedded fibers can survive the large stresses that result from differential thermal expansion between the glass fiber and the surrounding metal matrix. This work shows how optical fibers have been successfully embedded in aluminum and copper alloys in both straight and curved channels with various bend radii. The embedded fibers have also survived heating to temperatures of 500°C and cooling to room temperature. This paper presents some of the experimental results including measured light attenuation resulting from embedding with and without bends and high-temperature testing.

Key Words: Embedded; fiber optics; sensors; in-pile

---

1 INTRODUCTION

Advanced nuclear fuels and materials are critical to both next-generation reactor technologies and improved accident-tolerant light water reactors [1-4]. Qualification and commercialization of new fuels and materials requires experimentally validated modelling and simulation tools to predict performance during irradiation. Traditionally, radiation-induced changes in microstructure, thermophysical properties, geometry, etc., were obtained using a "cook-and-look" approach where fuels and materials were examined post-irradiation. This approach is both time-consuming and costly, with some experiments requiring months to years of design, irradiation, and post-irradiation examination to achieve a single data point on irradiation performance. Today, instrumented irradiation experiments use sensors that provide reasonably accurate measurements of temperature and neutron fluence; however, data regarding the in-situ performance of test specimens is very limited [5].

This paper describes work being performed at Oak Ridge National Laboratory to develop advanced fiber-optic sensors that can be embedded into in-core irradiation experiments in test reactors and perhaps some components in commercial reactors. Several previous works have demonstrated acceptable performance of fiber optics in-core and at very high temperatures [6-18]. Combining the embedding capabilities of ultrasonic additive manufacturing (UAM) [19-24] with fiber-optic sensing technologies could enable entirely new measurement techniques capable of surviving the harsh environment of a nuclear reactor. These new sensing techniques will help accelerate the time frame for development and deployment of advanced nuclear fuels and materials by providing high-fidelity real-time data for validation of nuclear fuel performance models. Optical fibers have been successfully embedded in aluminum and copper alloys in both straight and curved channels and survived heating to temperatures of 500°C. This paper will discuss measured light attenuation during this testing as well as plans to measure radial dimensional change and spatially distributed temperature and strain during irradiation.

2 EXPERIMENTAL APPROACH

2.1 Distributed Fiber-Optic Measurements

Spatially distributed measurements of the reflected light signal intensity can be made using optical frequency domain reflectometry (OFDR) [25-27]. The basic principle relies on the interference pattern produced from a reference leg (coupled directly from the light source to the detectors) and from backscatter reflections that occur along the entire length of a measurement leg. A tunable laser is used to sweep over a range of light frequencies. The optical path length difference depends on the location from which the reflection occurs. In this way, the photodetectors measure the superposition of all reflections occurring along the length of the fiber. Performing a Fourier transform on the measured intensity-vs-frequency data gives a reflected amplitude as a function of time delay, which of course can be related to the location (or position) from which the reflection occurred. When the fiber is locally heated or mechanically strained compared to some reference state, the spectral signature of the backscattered reflections is shifted. A spatially distributed sensor can be formed by windowing the intensity-vs-position data over the spatial range of interest, transforming that data back into the optical frequency domain, and performing a cross-correlation of the spectra compared with the reference measurement. The spectral shift that is determined from the cross-correlation can be calibrated to a change in temperature or strain. More details can be found in other publications [15, 28, 29].

2.2 Ultrasonic Additive Manufacturing and Fiber Embedding

UAM is a tape-layering process by which thin layers of metal are bonded together by a combination of pressure and ultrasonic motion. A vibrating tool, or sonotrode, creates a scrubbing motion that breaks down the surface oxides on the foil and the substrate. After adding layers, channels, or slots, can be machined in a component, and other materials, including sensors, can be placed inside the slot. Applying additional

layers results in components and/or sensors that are embedded within the part. Using UAM to embed sensors is especially attractive because it is a low-temperature process (<100°C when embedding in aluminum [30]).

2.3 High-Temperature Testing

As mentioned previously, one of the unresolved issues with embedded fiber-optic sensors is whether the fibers can survive high temperatures and the resulting differential thermal expansion between the fused silica fiber and the aluminum matrix. To address this issue, embedded fibers were placed inside a high-temperature oven and heated in steps to nominal temperatures of 100, 200, 300, 400, and 500°C, as monitored by a K-type thermocouple. Each temperature was held for approximately 15−20 minutes. After the final heating step, the furnace temperature was gradually cooled to room temperature. The fibers were interrogated throughout the experiment to monitor light transmission.

3 RESULTS

3.1 Embedding of Metallized Optical Fibers

All fibers embedded with a slot depth of less than 152 μm failed to transmit light after embedding. After coating, the fiber diameter is nominally 165 μm. Two examples of optical microscopy of copper-coated fibers embedded in aluminum are shown in Figure 1. Figure 1 shows that even though the embedded fiber with a slot depth of 152 μm had adequate light transmission, there was significant coating deformation after embedding. These results indicate that the slot depth should be greater than the fiber diameter after coating to achieve adequate bonding to the matrix without significant coating deformation.

Figure 2 shows an example of reflected signal amplitude as a function of position for a copper-coated fiber embedded in aluminum with a slot depth of 178 μm. The units of the signal amplitude are dB, with a reference intensity determined during a calibration scan performed with a highly reflective gold-coated fiber. The fiber is terminated with a core-less fiber near 16.27 m, which results in a large reflection. A smaller reflection occurs at 16.30 m at the interface between the end of the core-less fiber and the surrounding air. There is essentially zero signal returned beyond the end of the core-less fiber.

The embedded region is also indicated in Figure 2. Some signal loss occurs due to the embedding process. However, comparing the insertion loss (i.e., the difference in signal intensity immediately before and after the embedded region) indicates that the total signal attenuation for a single pass through the embedded region is only 1.1 dB. The results presented here for a fiber embedded in a straight channel can be compared with results presented in Section 3.2 for fibers embedded in curved channels with various bend radii.

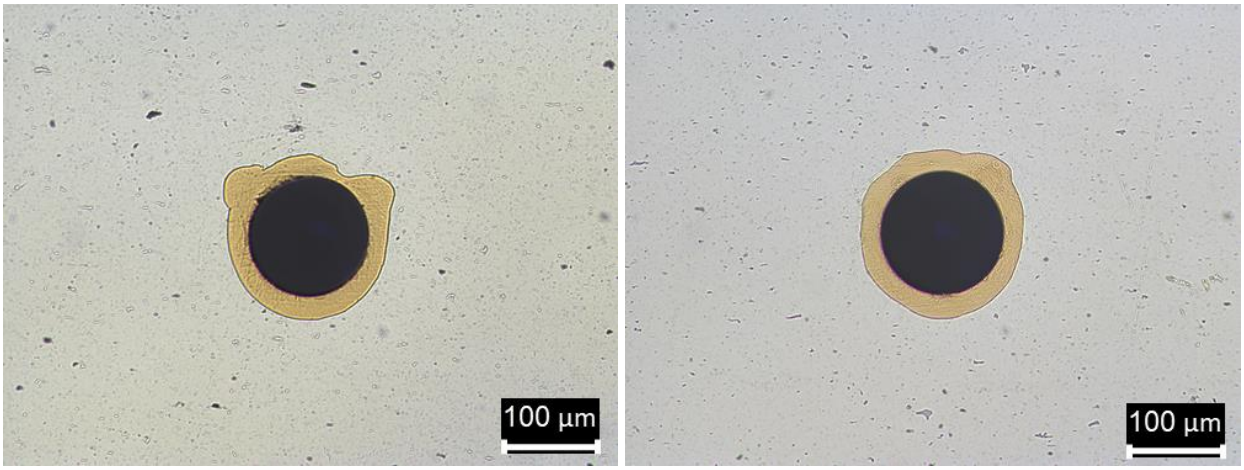

Figure 1. Optical microscopy of copper-coated fibers embedded in aluminum with slot depths of 152 µm (left) and 178 µm (right).

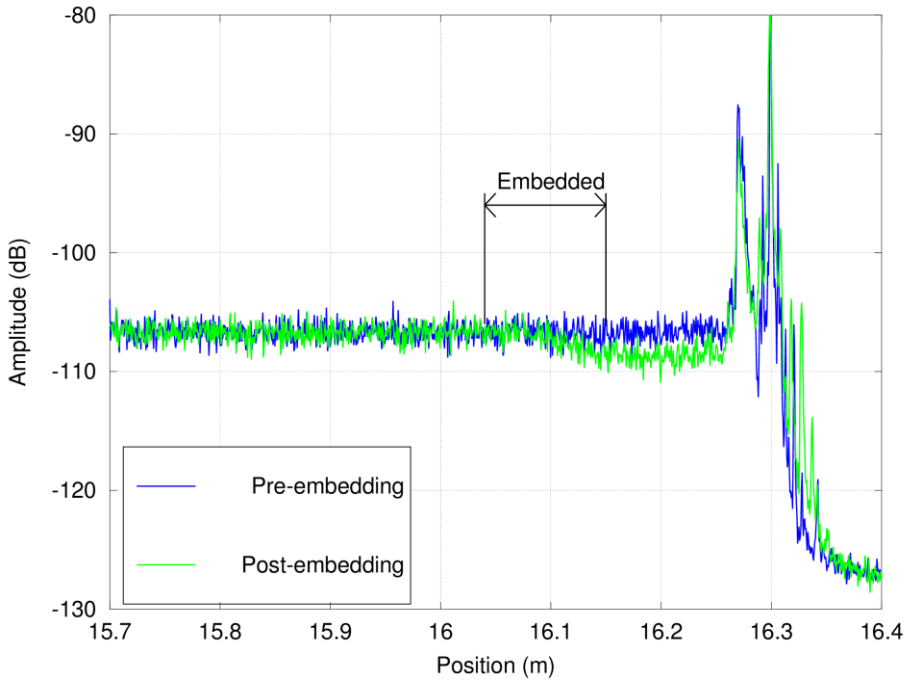

Figure 2. Reflected signal amplitude vs position for a copper-coated fiber embedded in a straight aluminum channel.

3.2 Embedding in Curved Channels

To use fiber optics to measure radial dimensional changes during irradiation, the fibers must pass down into an experiment vehicle and bend 90° so that the end of the fiber is pointed directly at the outer radial surface of the specimen. A schematic representation of this type of measurement is shown in Figure 3.

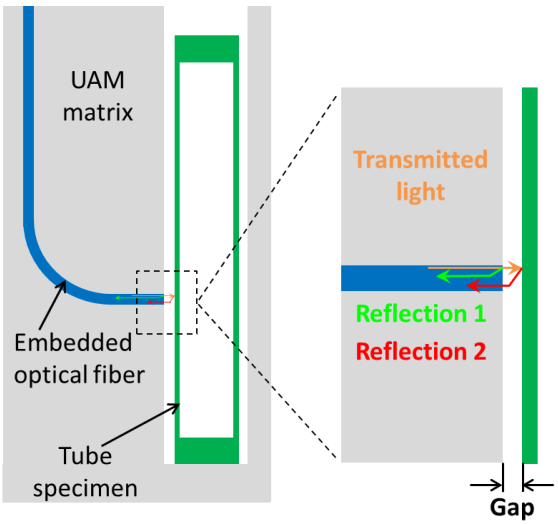

Figure 3. Schematic of potential measurement of radial dimensional change.

The diameter can be determined from the radial gap between the end of the fiber (flush with the surface of the UAM matrix) and the outer surface of the specimen. This gap is determined based on the interference pattern produced from two signals: (1) light that is reflected at the end of the embedded optical fiber and passes back through the same fiber toward a detector and (2) light that is transmitted beyond the first reflection, reflected off the outer surface of the specimen, and then passes back through the fiber toward a detector. Embedding the fiber in a curved channel allows for measurements of dimensional change without the use of epoxy, which would not survive for extended durations during irradiation. However, because of the limited size of typical irradiation vehicles, the fiber must be bent at a relatively small radius.

Experiments were performed to determine the limiting bend radius for embedded fibers by embedding fibers at three different radii: 6.35, 7.62, and 12.70 mm. These radii were determined based on the minimum recommended bending radius of 10 mm specified by the fiber manufacturer (IVG Fiber). One sample was tested for each bend radius. Figure 4 through Figure 6 show measured light intensity vs position for the three different bend radii. The insertion loss was calculated for a single pass through each of the bends as was done for the data in Figure 2 without a bend. Table I summarizes the insertion loss for all the data that were analyzed. The slightly larger insertion loss for the 12.70 mm radius bend compared to the loss for the 7.62 mm radius bend could be explained by small variations in the slot depth. The start of the bend can be easily identified in Figure 5 (near 15.17 m) and Figure 6 (near 16.2 m); the start of the bend is not as clear in Figure 4 (perhaps near 15.2 m). Based on these results, the fiber can successfully transmit light with a bend radius as small as 6.35 mm.

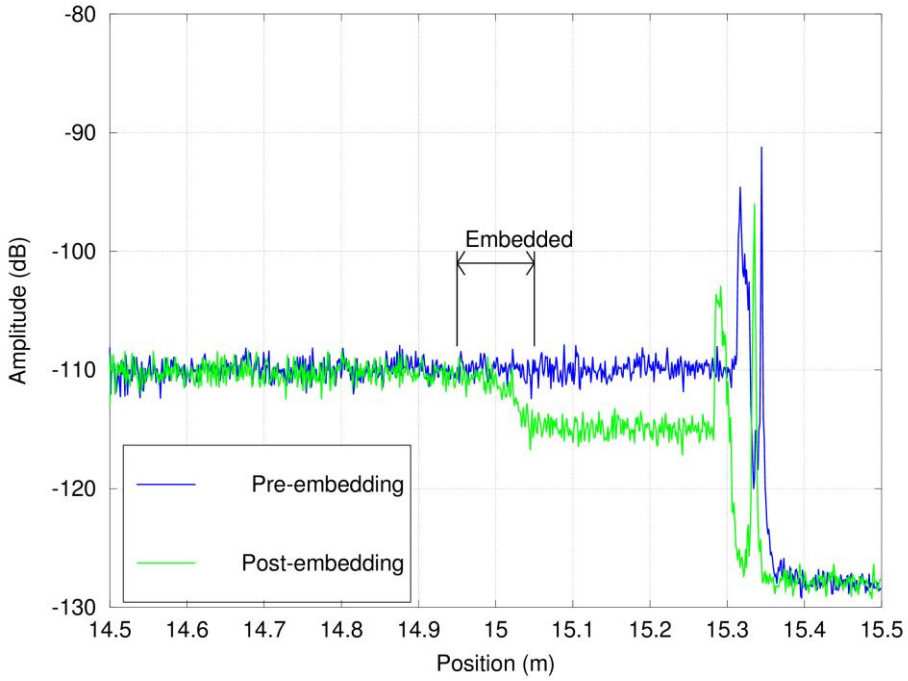

Figure 4. Amplitude vs position after embedding in channel with 12.70 mm bend radius.

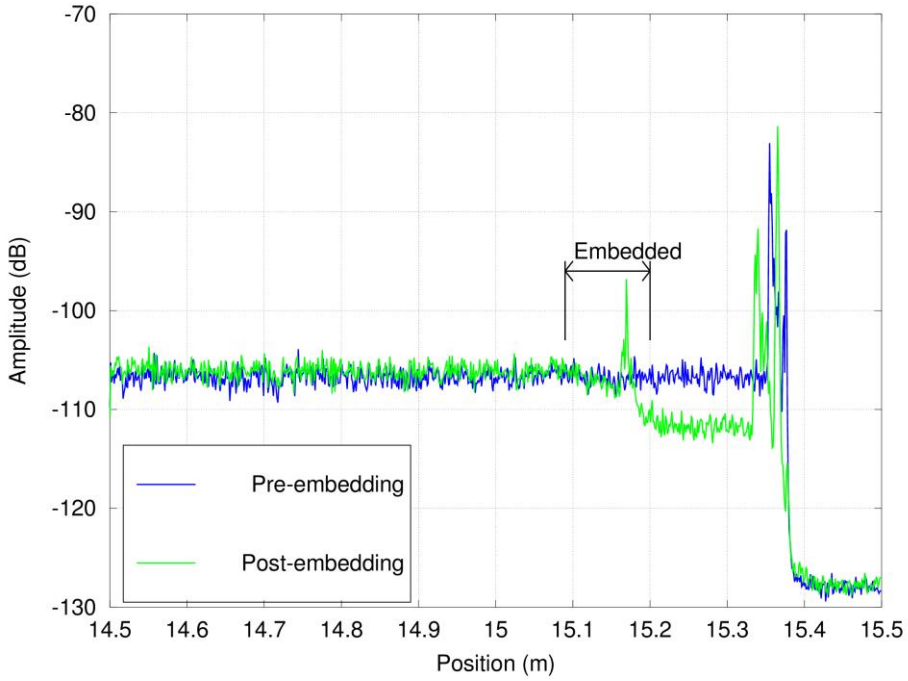

Figure 5. Amplitude vs position after embedding in channel with 7.62 mm bend radius.

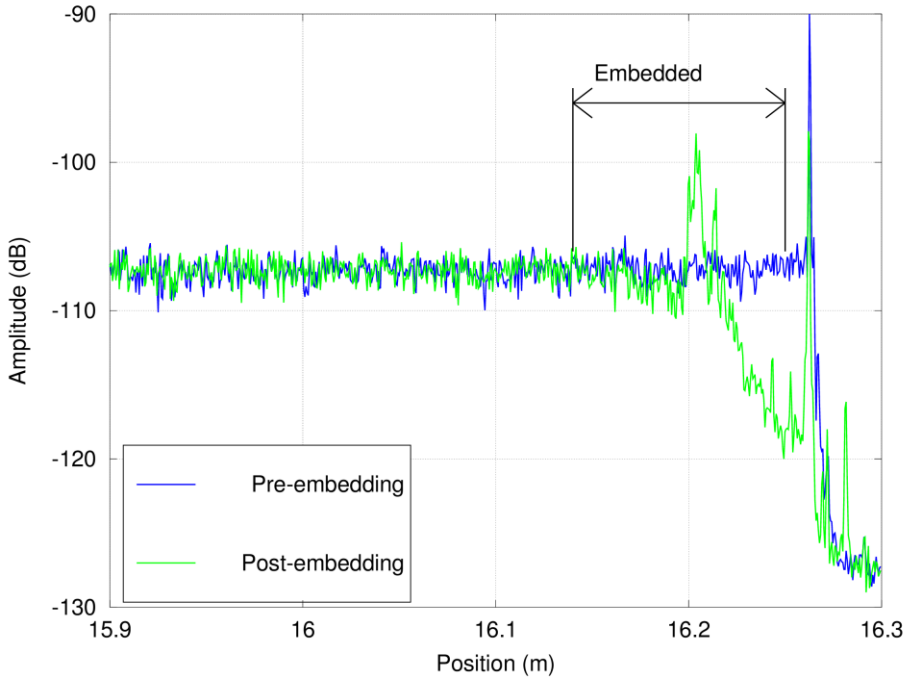

Figure 6. Amplitude vs position after embedding in channel with 6.35 mm bend radius.

Table I. Return loss for all samples

Channel bend	Insertion loss for a single pass (dB)	Embedded length (mm)	Insertion loss for a single pass (dB/m)
None	1.1	110	10
12.70 mm radius	2.4	100	24
7.62 mm radius	2.4	110	22
6.35 mm radius	5.0	110	45

3.3 High-Temperature Testing

Embedded fibers were heated to temperatures as high as 500°C to determine whether they could survive differential thermal expansion between the fused silica fiber and the surrounding aluminum matrix. Figure 7 shows temperature and the signal amplitude at the end of the embedded region as a function of time throughout the experiment. Results are shown for an aluminum-coated fiber embedded in a straight aluminum channel. Figure 7 shows that the signal intensity improves as the embedded fiber is heated. The exact mechanism for the improved signal intensity is not clear. Because the improvement in signal intensity generally remained after cooling, the explanation for the improved signal intensity could be related to partial annealing of residual stresses that developed after embedding. Residual stress after embedding can cause reductions in signal intensity, as shown in Figure 2. In any case, the results shown in Figure 7 clearly show that the fiber survived heating to temperatures greater than 500°C and the resulting thermal strain.

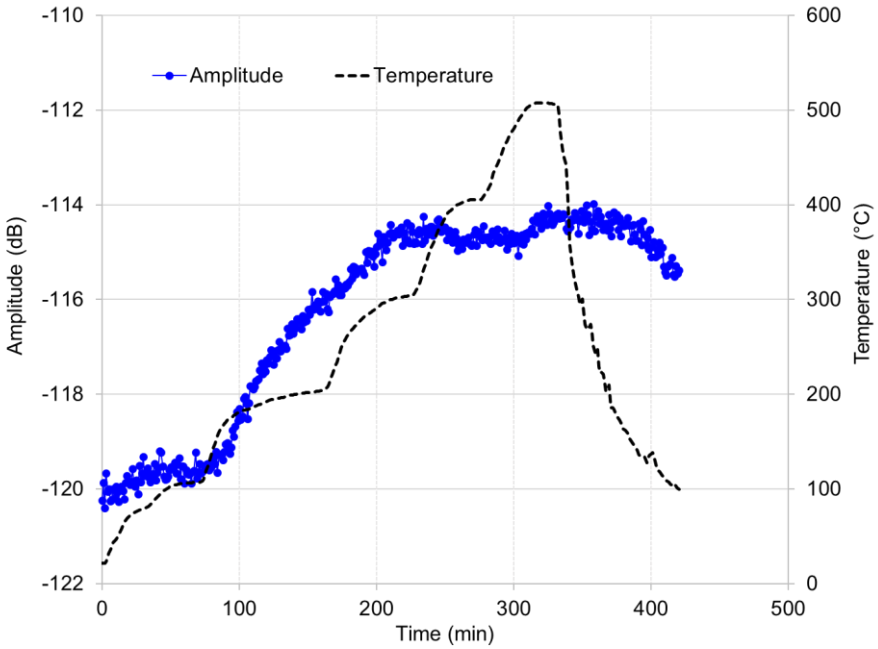

Figure 7. Temperature and amplitude near the end of the embedded region as a function of time during heating.

The expected differential thermal strain can be calculated using known thermal expansion data for fused silica and aluminum. Using data from the CINDAS database [31], the expected thermal strains for fused silica and aluminum at 500°C are 0.027% and 1.32%, respectively. The resulting differential thermal strain is 1.29%. For fused silica with an elastic modulus of 73 GPa, the resulting stress is 944 MPa. Previous work has shown that short lengths of optical fibers can have extremely high tensile strengths, with some values as high as 14 GPa [32]. Therefore, it is not surprising that the fiber was able to survive such extreme thermal strain. The fiber itself can be used to measure strain during heating. While the in-situ strain measurements are discussed in detail in a separate publication [33], it is worth noting here that, including thermo-optic effects, the measured strain in the embedded region at 500°C was approximately 1.7%. The strain due to thermo-optic effects in fused silica at 500°C is approximately 0.4% [34]. Therefore, the measured strain of 1.7% can be compared with the expected strain of 1.29% + 0.4% = 1.69%. This excellent agreement shows that the fiber is indeed bonded to the surrounding aluminum matrix and that the shear strength at the fiber/coating interface and the coating/matrix interface exceeds the estimated thermal stress of 944 MPa.

4 SUMMARY

This paper summarizes some initial work that has been done to develop embedded fiber-optic sensors for in-pile applications. The goal of this project is to use embedded fiber-optic sensors for measuring spatially distributed temperature and strain and to use embedded fibers to measure radial dimensional change. This paper describes work that was done to embed metallized optical fibers in aluminum using UAM, including evaluating the proper depth of the slot in which the fiber is set prior to embedding. Embedding in curved channels was also evaluated. It was found that light could be successfully transmitted for bend radii as small as 6.35 mm, although reflections were observed near the location of the bend at bend radii of 7.62 and 6.35 mm. Finally, embedded fibers were heated to temperatures as high as 500°C to determine whether the fiber could survive the strain that results from differential thermal expansion between the fused silica fiber and the surrounding aluminum matrix. Despite expected thermal strains of 1.2%, the fiber survived heating to 500°C and cooling to room temperature.

5 ACKNOWLEDGMENTS

This research is sponsored by the Laboratory Directed Research and Development Program of Oak Ridge National Laboratory (ORNL), managed by UT-Battelle, LLC, for the US Department of Energy.

6 REFERENCES

1. K. A. Terrani, "Accident tolerant fuel cladding development: Promise, status, and challenges," *Journal of Nuclear Materials*, **501**, pp. 13-30 (2018).
2. S. J. Zinkle, K. A. Terrani, J. C. Gehin, L. J. Ott, L. L. Snead, "Accident tolerant fuels for LWRs: A perspective," *Journal of Nuclear Materials*, **448**, pp. 374–379 (2014).
3. S. J. Zinkle, G. S. Was, "Materials challenges in nuclear energy," *Acta Materialia*, **61**, pp. 735-758 (2013).
4. S. J. Zinkle, J. T. Busby, "Structural materials for fission & fusion energy," *Materials Today*, **12**, pp. 12-19 (2009).
5. B. G. Kim, J. L. Rempe, J.-F. Villard, S. Solstad, "Review Paper: Review of Instrumentation for Irradiation Testing of Nuclear Fuels and Materials," *Nuclear Technology*, **176**, pp. 155-187 (2011).
6. G. Cheymol, H. Long, J. F. Villard, B. Brichard, "High Level Gamma and Neutron Irradiation of Silica Optical Fibers in CEA OSIRIS Nuclear Reactor," *IEEE Transactions on Nuclear Science*, **55**, pp. 2252-2258 (2008).
7. G. Cheymol, A. Gusarov, S. Gaillot, C. Destouches, N. Caron, "Dimensional measurements under high radiation with optical fibre sensors based on white light interferometry - report on irradiation tests," *2013 3rd International Conference on Advancements in Nuclear Instrumentation, Measurement Methods and their Applications*, Marseille, France, 2013, pp. 1-7 (2013).
8. L. Remy, G. Cheymol, A. Gusarov, A. Morana, E. Marin, S. Girard, "Compaction in Optical Fibres and Fibre Bragg Gratings Under Nuclear Reactor High Neutron and Gamma Fluence," *IEEE Transactions on Nuclear Science*, **63**, pp. 2317–2322 (2016).
9. D. P. Hawn, C. M. Petrie, T. E. Blue, W. Windl, "In-situ gamma radiation induced attenuation in silica optical fibers heated up to 600°C," *Journal of Non-Crystalline Solids*, **379**, pp. 192-200 (2013).
10. C. M. Petrie, D. P. Hawn, W. Windl, T. E. Blue, "Reactor radiation-induced attenuation in fused silica optical fibers heated up to 1000 °C," *Journal of Non-Crystalline Solids*, **409**, pp. 88–94 (2015).
11. C. M. Petrie, B. Wilson, T. E. Blue, "In Situ Gamma Radiation-Induced Attenuation in Sapphire Optical Fibers Heated to 1000°C," *Journal of the American Ceramic Society*, **97**, pp. 3150-3156 (2014).
12. C. M. Petrie, W. Windl, T. E. Blue, "In-Situ Reactor Radiation-Induced Attenuation in Sapphire Optical Fibers," *Journal of the American Ceramic Society*, **97**, pp. 3883–3889 (2014).
13. C. M. Petrie, T. E. Blue, "In situ reactor radiation-induced attenuation in sapphire optical fibers heated up to 1000 °C," *Nuclear Instruments and Methods in Physics Research Section B: Beam Interactions with Materials and Atoms*, **342**, pp. 91–97 (2015).
14. B. A. Wilson, C. M. Petrie, T. E. Blue, "High-temperature effects on the light transmission through sapphire optical fiber," *Journal of the American Ceramic Society*, **101**, pp. 3452-3459 (2018).
15. T. W. Wood, B. Blake, T. E. Blue, C. M. Petrie, D. Hawn, "Evaluation of the Performance of Distributed Temperature Measurements with Single-Mode Fiber Using Rayleigh Backscatter up to 1000°C," *IEEE Sensors Journal*, **14**, pp. 124-128 (2014).
16. B. A. Wilson, T. E. Blue, "Quasi-distributed Temperature Sensing using Type-II Fiber Bragg Gratings in Sapphire Optical Fiber to Temperatures up to 1300°C," *IEEE Sensors Journal* (in press).
17. R. S. Fielder, D. Klemer, K. L. Stinson-Bagby, "High Neutron Fluence Survivability Testing of Advanced Fiber Bragg Grating Sensors," *AIP Conference Proceedings*, **699**, pp. 650-657 (2004).

18. M. A. S. Zaghloul, M. Wang, S. Huang, C. Hnatovsky, D. Grobnic, S. Mihailov, M.-J. Li, D. Carpenter, L.-W. Hu, J. Daw, G. Laffont, S. Nehr, K. P. Chen, "Radiation resistant fiber Bragg grating in random air-line fibers for sensing applications in nuclear reactor cores," *Optics Express*, **26**, pp. 11775-11786 (2018).
19. A. Hehr, M. Norfolk, J. Wenning, J. Sheridan, P. Leser, P. Leser, J. A. Newman, "Integrating Fiber Optic Strain Sensors into Metal Using Ultrasonic Additive Manufacturing," *Journal of The Minerals, Metals & Materials Society*, **70**, pp. 315-320 (2018).
20. C. Y. Kong, R. Soar, "Method for embedding optical fibers in an aluminum matrix by ultrasonic consolidation," *Applied Optics*, **44**, pp. 6325–6333 (2005).
21. J. J. Schomer, M. J. Dapino, "High Temperature Characterization of Fiber Bragg Grating Sensors Embedded Into Metallic Structures Through Ultrasonic Additive Manufacturing," *ASME 2017 Conference on Smart Materials, Adaptive Structures and Intelligent Systems*, Snowbird, Utah, USA, 2017, Vol. 2, pp. V002T005A003 (2017).
22. J. J. Schomer, A. J. Hehr, M. J. Dapino, "Characterization of embedded fiber optic strain sensors into metallic structures via ultrasonic additive manufacturing," *SPIE Smart Structures and Materials + Nondestructive Evaluation and Health Monitoring*, Las Vegas, Nevada, USA, 2016, Vol. 9803, pp. 980320 (2016).
23. T. Monaghan, A. J. Capel, S. D. Christie, R. A. Harris, R. J. Friel, "Solid-state additive manufacturing for metallized optical fiber integration," *Composites Part A: Applied Science and Manufacturing*, **76**, pp. 181–193 (2015).
24. Y. Li, W. Liu, Y. Feng, H. Zhang, "Ultrasonic embedding of nickel-coated fiber Bragg grating in aluminum and associated sensing characteristics," *Optical Fiber Technology*, **18**, pp. 7–13 (2012).
25. M. Froggatt, B. Soller, D. Gifford, M. Wolfe, "Correlation and keying of Rayleigh scatter for loss and temperature sensing in parallel optical networks," *Optical Fiber Communication Conference*, Los Angeles, California, USA, 2004, pp. PDP17 (2004).
26. B. J. Soller, M. Wolfe, M. E. Froggatt, "Polarization Resolved Measurement of Rayleigh Backscatter in Fiber-Optic Components," *Optical Fiber Communication Conference and Exposition and The National Fiber Optic Engineers Conference*, Anaheim, California, USA, 2005, pp. NWD3 (2005).
27. B. J. Soller, D. K. Gifford, M. S. Wolfe, M. E. Froggatt, "High resolution optical frequency domain reflectometry for characterization of components and assemblies," *Optics Express*, **13**, pp. 666–674 (2005).
28. M. E. Froggatt, D. K. Gifford, S. T. Kreger, M. S. Wolfe, B. J. Soller, "Distributed Strain and Temperature Discrimination in Unaltered Polarization Maintaining Fiber," *Optical Fiber Sensors*, Cancun, Mexico, 2006, pp. ThC5 (2006).
29. S. T. Kreger, D. K. Gifford, M. E. Froggatt, A. K. Sang, R. G. Duncan, M. S. Wolfe, B. J. Soller, "High-resolution extended distance distributed fiber-optic sensing using Rayleigh backscatter," *Proceedings of SPIE*, San Diego, California, USA, 2007, Vol. 6530, pp. 65301R (2007).
30. M. R. Sriraman, M. Gonser, D. Foster, H. T. Fujii, S. S. Babu, M. Bloss, "Thermal Transients During Processing of 3003 Al-H18 Multilayer Build by Very High-Power Ultrasonic Additive Manufacturing," *Metallurgical and Materials Transactions B*, **43**, pp. 133–144 (2012).
31. "CINDAS, LLC: Global Benchmark for Critically Evaluated Materials Properties Data," http://cindasdata.com (2016).
32. R. Olshansky, R. D. Maurer, "Tensile strength and fatigue of optical fibers," *Journal of Applied Physics*, **47**, pp. 4497-4499 (1976).
33. C. M. Petrie, N. Sridharan, J. Sheridan, A. Hehr, M. Norfolk, S. S. Babu, "Embedded metallized optical fibers for high temperature applications," *Smart Materials and Structures* (in preparation).
34. K. O. Hill, G. Meltz, "Fiber Bragg grating technology fundamentals and overview," *Journal of Lightwave Technology*, **15**, pp. 1263-1276 (1997).